Available online at www.sciencedirect.com
ScienceDirect
Trans. Nonferrous Met. Soc. China 34(2024) 2304−2312
Transactions of Nonferrous Metals Society of China
www.tnmsc.cn

Predictive model of corrosion kinetics for lead-free solder in polyvinyl chloride fire smoke environment

Qian LI, Jin LIN, Meng-ke ZHAO, Chang-hai LI, Shou-xiang LU

State Key Laboratory of Fire Science, University of Science and Technology of China, Hefei 230026, China

Received 16 January 2023; accepted 18 July 2023

Abstract: The corrosion kinetics, surface microstructure, and corrosion mechanism of Sn−3.0Ag lead-free solder were investigated using mass-loss method in the temperature range from 283.15 to 323.15 K in polyvinyl chloride fire smoke environment. The results show that the Sn−3.0Ag solder exhibits an increase in mass-loss from (22.09±2.01) to (44.66±1.20) g/m^2 as the temperature increases from 283.15 to 323.15 K. Moreover, the corrosion kinetics is in accordance with Arrhenius law. The surface corrosion products of Sn−3.0Ag solder show a superposition growth trend. At 283.15 K, the surface of Sn−3.0Ag solder shows significant corrosion products. The corrosion process of Sn−3.0Ag lead-free solder is an electrochemical corrosion. Hydrogen evolution and oxygen abstraction reactions occur in the cathode, and the dissolution of the Sn-rich phase occurs in the anode. The corrosion products are $Sn_{21}Cl_{16}(OH)_{14}O_6$, SnO_2, and SnO.

Key words: corrosion; predictive model; Sn−3.0Ag solder; fire smoke; temperature

1 Introduction

As the interconnection material of electronic devices, tin solder is widely used in the chip packaging, which is critical for electronic device reliability [1−4]. With the miniaturization, multi-function, high-power, and high-integration of electronic devices, the electrical, thermal, and mechanical loads carried by the solder joints on packaging are becoming more serious, making them more sensitive to environmental corrosion [5,6]. Sn−Pb solder has been widely used as a traditional tin solder [7,8]. However, owing to the toxicity of Pb to the human body and the harm to the environment, domestic and international regulations are enacted to ban the application of the lead solders [9−12]. Lead-free solders are already excellent and popular candidates in the market, among which Sn−3.0Ag solder, as a basic binary alloy solder, has also been widely studied [13−15]. However, lead-free solders have a lower corrosion resistance than lead-based solders [16,17]. Therefore, the reliability challenge for electronic packaging is becoming more and more serious.

With the rapid development of electric power, the fire caused by cable aging easily leads to damage and failure of electronic devices. The fire damage is mainly manifested as thermal damage and non-thermal damage. Thermal damage is caused by heat in the process of fire. Non-thermal damage refers to the damage caused by smoke, pollutant ions, and water vapor during the firing process without obvious temperature rising [18]. In unburned areas, electronic devices and facilities often suffer non-thermal damage rather than thermal damage, which is prone to corrosion due to smoke sedimentation and fire water action, reducing

Corresponding author: Jin LIN, Tel: +86-551-63607881, E-mail: linjin@ustc.edu.cn;
Shou-xiang LU, Tel: +86-551-63603141, E-mail: sxlu@ustc.edu.cn
DOI: 10.1016/S1003-6326(24)66542-8

their reliability [19]. Tin solder, in particular, is more vulnerable to corrosion, making it prone to failure. Thus, the corrosion behavior of tin solder in the fire smoke environment is of concern.

Currently, the focus on the corrosion behavior of tin solder lies primarily on its reliability in the marine environment. Salt spray tests are carried out to simulate the marine environment [20−22], and few studies are focused on its corrosion behavior in acidic solution [23,24]. Besides, most studies are focused on the effect of element content and addition on the corrosion behavior of tin solder. The results show that the corrosion resistance of Sn−3.0Ag solder is poor and it is prone to significant corrosion in neutral salt spray solution. The corrosion tests of Sn−Ag and Sn−Cu solders carried out by YOKOYAMA et al [21] show that Sn−3.0Ag solder is more prone to creep corrosion cracking damage than Sn−0.5Cu solder in NaCl neutral solution. SHARMA et al [25] compare the corrosion behavior of Sn−Ag with Sn−Ag/CeO_2 solder in 3.5% NaCl solution. The results show that Sn−Ag solder exhibits poor corrosion resistance than Sn−Ag/CeO_2 solder because the corrosion products on the surface are coarser and looser, inhibiting corrosion weakly compared to the finer corrosion products on the surface of Sn−Ag/CeO_2 solder. HEAKAL et al [23] contrastively analyze the corrosion behavior of Sn−3.0Ag solder with different tin additions (26%, 50%, 70%, and 96.5%) in nitric acid solution. The research findings indicate that at lower acid concentrations, the corrosion behavior of solders becomes more severe as the acid concentration increases, particularly for solders with lower tin contents (26% and 50%) exhibiting more pronounced corrosion behavior. However, at higher acid concentrations, all solders exhibit the same corrosion behavior.

Temperature plays a fundamental role in determining the corrosion degree of solder [26]. Nevertheless, few studies are carried out to investigate the effect of temperature on the corrosion behavior of Sn−3.0Ag solder. Therefore, we innovatively reproduce the smoke environment with different temperatures after the fire, and systematically research the influence of different temperatures on the corrosion behavior of Sn−3.0Ag lead-free solder in PVC fire smoke environment. In this work, the commonly used wire and cable sheath insulation material, polyvinyl chloride (PVC), is used as fuel to generate fire smoke [27]. The corrosion degree of Sn−3.0Ag lead-free solder in a fire smoke environment is evaluated by the mass-loss method. The predictive model for corrosion kinetics of Sn−3.0Ag solder is built in the temperature range of 283.15−323.15 K. Besides, the surface corrosion microstructure and corrosion products are analyzed by different physicochemical characterization techniques. The corrosion mechanism of Sn−3.0Ag solder is revealed in PVC fire smoke environment. Grasping the corrosion behavior of Sn−3.0Ag solder in fire smoke environment at different temperatures can guide the assessment of electronic devices damage after a fire accident, to make a better rescue plan.

2 Experimental

2.1 Materials and methods

The sample studied in this experiment is Sn−3.0Ag lead-free solder (composition: Sn 97.0 wt.%, Ag 3.0 wt.%) with dimensions of (75±0.12) mm (length) × (25±0.03) mm (width) × (1±0.001) mm (height). PVC, as the raw material of wire and cable, is used as fuel to generate fire smoke. The mass-loss method was adopted to study the influence of temperature on the corrosion behavior of Sn−3.0Ag solder in PVC fire smoke environment due to the complicacy of fire smoke components, which were challenging to simulate as an electrolyte solution. Before the test, Sn−3.0Ag solder was polished with different mesh sandpaper successively, rinsed with deionized water and alcohol, and then blown dry with air and keeping in a drying bottle for at least one day. The size was measured and the mass of all samples was weighed. For accuracy, four samples were placed in each group of test conditions. One sample was used to analyze the corrosion microstructure and corrosion products of solder. The other three samples were used to analyze the corrosion kinetics. All the three samples were immersed in 0.15 g/mL trisodium phosphate solution for 10 min after corrosion test according to the ISO 8407, and then the surface corrosion products were removed with an eraser. In addition, blank samples were used for correction. The mass-loss of Sn−3.0Ag solder was used to characterize corrosion kinetics, which could be inferred as follows [28−30]:

$$W=\frac{m_0-m_{\mathrm{i}}+m_{\mathrm{b0}}-m_{\mathrm{b1}}}{s} \tag{1}$$

where W is the mass-loss (g/m^2); m_0 is the initial mass (g) of tested samples before the smoke corrosion test; m_{b0} is the initial mass (g) of blank contrast samples before the smoke corrosion test; m_i is the mass (g) of tested samples after the treatment; m_{b1} is the mass (g) of blank contrast samples after the treatment; s is the sample surface area (m^2).

2.2 Experimental setup

The experimental device is referred to by our previous work, as shown in Fig. 1 [31]. The experimental device consists of a tubular furnace, a smoke corrosion chamber, and a data acquisition system. PVC powder is burned in a tubular furnace, the inlet air-flow rate is 5 L/min and the dosage of PVC powder is 14.7 g. The generated fire smoke passed into the fire smoke corrosion chamber, and the corrosion test was carried out for up to 48 h. A small fan was placed at the bottom of the chamber to ensure uniform distribution of smoke during smoke production, and a quartz crystal micro-balance was used to monitor the smoke settlement process. A smoke corrosion chamber could control the temperature and relative humidity. The researched temperatures were 283.15, 293.15, 303.15, 313.15, and 323.15 K, respectively.

2.3 Characterization

Field emission scanning electron microscopy (FESEM) on a Philips SIRION 200 instrument was used to analyze surface corrosion microstructure, and elemental analysis was carried out on a Philips energy dispersive X-ray spectrometer (EDS). Philips X-ray diffraction (XRD) was employed to analyze the crystalline phase constitutions. Elemental composition and element valence states were researched by the X-ray photoelectron spectroscopy (XPS) on an Thermo-VG Scientific ESCALAB 250 spectrometer.

3 Results and discussion

3.1 Corrosion kinetics

To research the influence of temperature on the corrosion kinetics of Sn−3.0Ag solder in PVC fire smoke environment, the mass-loss variation of Sn−3.0Ag solder in PVC fire smoke environment with different temperatures is analyzed, as shown in Fig. 2. The results show that as the temperature increases from 283.15 to 323.15 K, the mass-loss of Sn−3.0Ag solder increases significantly from (22.09±2.01) to (44.66±1.20) g/m^2. This indicates that temperature promotes the corrosion of Sn−3.0Ag solder. With increasing temperature, the electrolyte resistance decreases and the diffusion rate accelerates. Consequently, the corrosion cell reacts more rapidly, leading to a faster corrosion progression.

To further investigate the corrosion kinetic, it is assumed that the mass-loss of Sn−3.0Ag follows the Arrhenius law:

$$W = A\exp(-\frac{E_a}{RT}) \tag{2}$$

where W depends on the temperature T (K), and activation energy E_a (kJ/mol). E_a characterizes the potential barrier that exists during the transition from non-corrosive to corrosive for tin solder. When the energy provided exceeds this barrier, the sample will enter the corrosion process. Therefore, it is an important indicator to reflect the corrosion degree of tin solder. The smaller the activation energy is, the easier the tin solder corrosion is. A is a parameter related to sample characteristics, geometry, test methods, models, etc. R is the molar gas constant (J·mol^{-1}·K^{-1}).

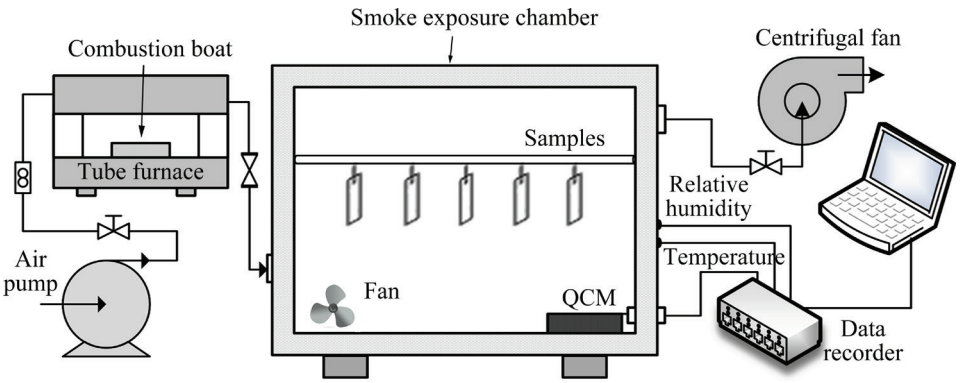

Fig. 1 Schematic diagram of experimental apparatus [31]

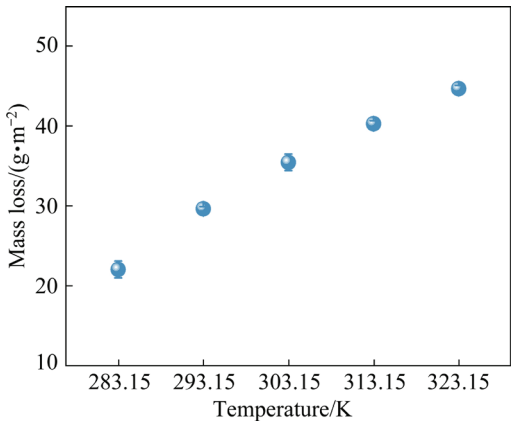

Fig. 2 Mass-loss variation of Sn−3.0Ag solder with temperature in PVC fire smoke environment

By taking the logarithm of each side of Eq. (2), the following equation is obtained:

$$\ln W = -\frac{E_a}{RT} + \ln A \tag{3}$$

Fitting curve in Fig. 3 depicts the relationship between mass loss and temperature. It can be observed that the r^2 of the fitting curve is 0.97, indicating that the curve fits well and the corrosion kinetics can be characterized by Arrhenius law. The parameters obtained from the fitting curve are given in Table 1. The value of E_a is 2.18×10^{-20} kJ/mol, and the value of A is 6221.09. Based on this model, the mass-loss of Sn−3.0Ag solder at different temperatures can be calculated approximately.

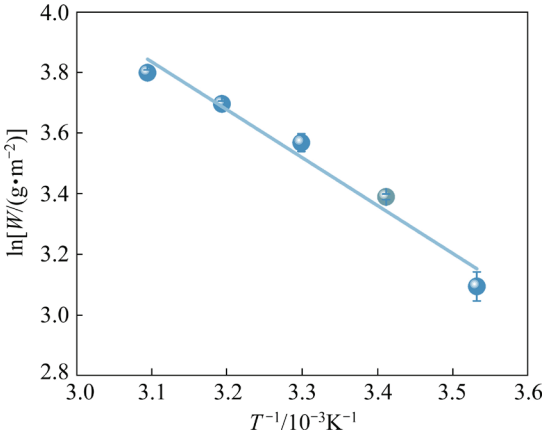

Fig. 3 Corrosion kinetic fitting curve of Sn−3.0Ag solder in PVC fire smoke environment

Table 1 Fitting parameters of corrosion kinetic curve of Sn−3.0Ag solder in PVC fire smoke environment

A	E_a/(kJ·mol^{-1})	r^2
6221.09	2.18×10^{-20}	0.97

3.2 Surface microstructure

Figure 4 exhibits the corrosion morphology of the corroded Sn−3.0Ag solder. Figure 4(a) shows the macroscopic morphology of the corroded sample. It can be observed that a layer of gray powder, which is corrosion product, appears on the surface of Sn−3.0Ag solder. Further, the optical microscopic morphology is shown in Fig. 4(b). The red circle indicates whiskers, which are corrosion products on the surface. It can be found that the surface of Sn−3.0Ag solder has been severely corroded, and a large number of corrosion products have appeared after fire smoke corrosion.

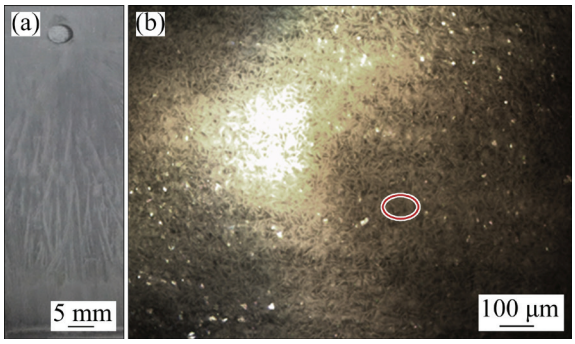

Fig. 4 Surface corrosion morphologies of Sn−3.0Ag solder after corrosion: (a) Macroscopic morphology; (b) Optical microscopic morphology

Figure 5 shows the surface microstructure of corrosion products on Sn−3.0Ag solder at 283.15, 293.15, 303.15, 313.15, and 323.15 K. Small patches of corrosion products are observed on the surface of Sn−3.0Ag solder at 283.15 K. Large corrosion products appear on the surface of Sn−3.0Ag solder, and the corrosion products are relatively thin at 293.15 K. When the temperature rises to 313.15 K, the corrosion products become very large but relatively sparse. At 323.15 K, the corrosion products densely and thickly cover Sn−3.0Ag solder surface. This indicates that with the increase of temperature, the corrosion products on Sn−3.0Ag solder surface become larger and thicker, indicating that higher temperatures favor the formation of corrosion product layer. The corrosion products increase firstly and then thicken in superposition growth mode. EDS analysis of Sn−3.0Ag solder corroded at 323.15 K shows that the surface corrosion products consist of three elements: Sn, Cl, and O.

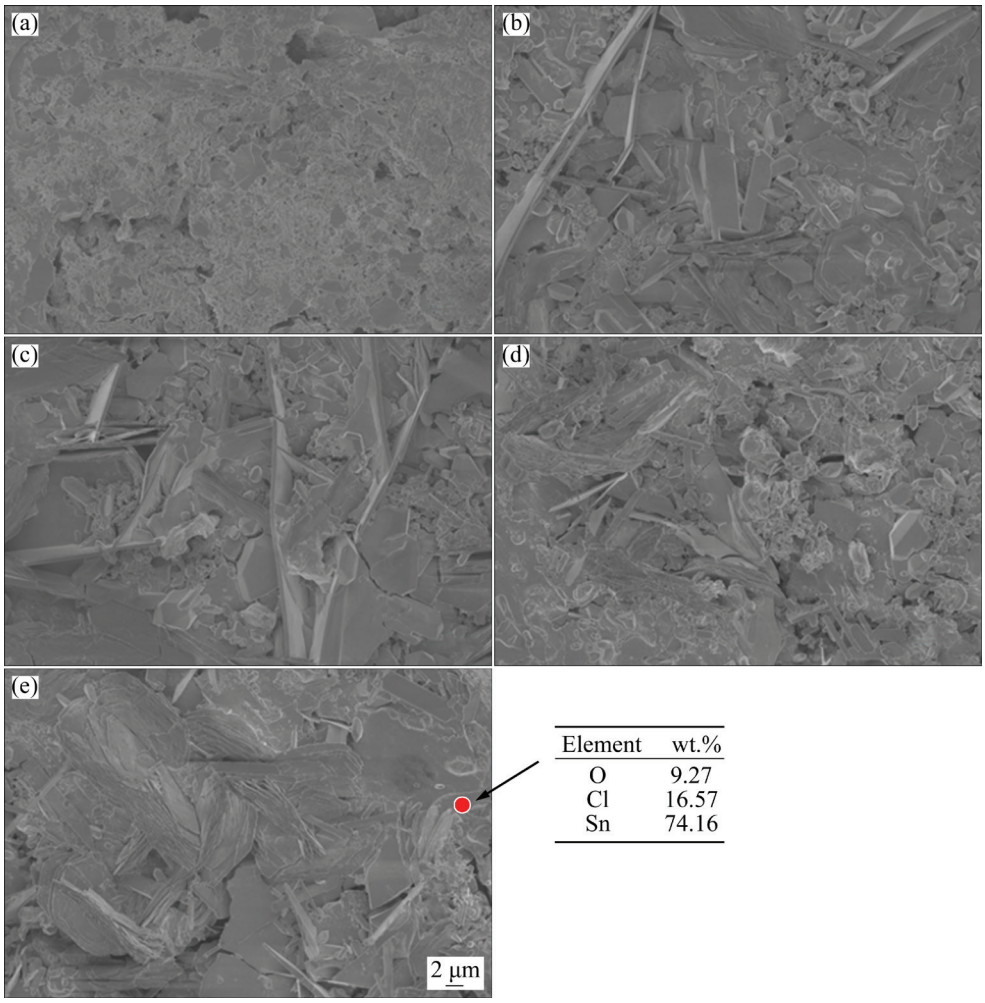

Fig. 5 Surface morphologies of corrosion products on Sn−3.0Ag solder in PVC fire smoke environment at different temperatures: (a) 283.15 K; (b) 293.15 K; (c) 303.15 K; (d) 313.15 K; (e) 323.15 K

3.3 Corrosion mechanism

To analyze the smoke corrosion mechanism of Sn−3.0Ag solder, XRD test is carried out on the corrosion products of Sn−3.0Ag solder at 323.15 K to identify the phase composition, and the test results are shown in Fig. 6. Compared with the PDF card library, the XRD diffraction peaks of Sn−3.0Ag solder correspond to $Sn_{21}Cl_{16}(OH)_{14}O_6$ (JCPDS No. 15-0676). The results show that the surface corrosion products of Sn−3.0Ag solder are mainly $Sn_{21}Cl_{16}(OH)_{14}O_6$.

To further analyze the composition of the corrosion products on the Sn−3.0Ag solder surface, XPS test is carried out on the surface substances of Sn−3.0Ag solder corroded in PVC fire smoke environment. Figure 7 shows the XPS full spectrum of corrosion products on Sn−3.0Ag solder at 323.15 K. It could be observed that Sn 3d, Sn 3p, Sn 4d, O 1s, Cl 2p, and C 1s are detected. The element content is given in Table 2. Among them, C is used to calibrate the peak position, and the other elements can be considered as the constituent elements of the corrosion products. The content of

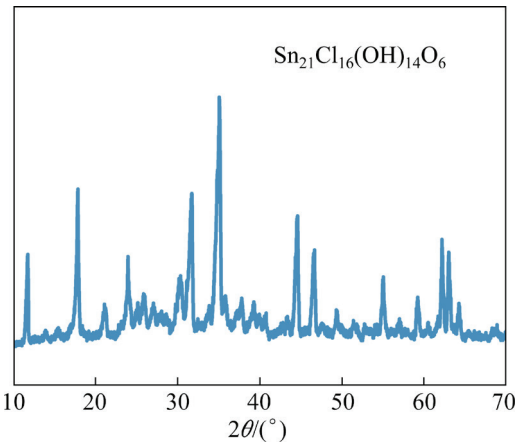

Fig. 6 XRD patterns of corrosion products of Sn−3.0Ag solder in PVC fire smoke environment at 323.15 K

O is the highest, followed by Sn, and the content of Cl is the lowest, indicating that the corrosion products mainly exist in the form of oxides. However, the contents of Ag are not detected, because the corrosion products are thicker and exceed the detection depth limit of XPS, which further indicates that Ag is not involved in the reaction.

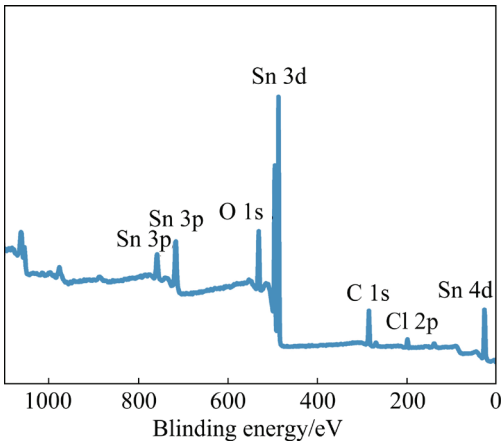

Fig. 7 XPS full spectrum of corrosion products for Sn−3.0Ag solder in PVC fire smoke environment at 323.15 K

Table 2 Element contents of XPS spectra for corrosion products of Sn−3.0Ag solder (at.%)

C 1s	O 1s	Sn 3d	Cl 2p
46.97	33.18	15.17	4.68

Peak processing is performed on the detected elements with XPS to further analyze the valence states of elements. The results are shown in Fig. 8, where Sn 3d can be decomposed in Sn^{2+} and Sn^{4+} at 486.6 and 487.1 eV, respectively [32]. O 1s is composed of O—Sn^{2+}/Sn^{4+} at 530.4 eV and O—OH at 531.7 eV [33,34]. Cl 2p is decomposed in two peaks at 198.2 and 199.7 eV for Cl^-. By combining the EDS and XRD results from the previous analysis, it could be considered that the main corrosion products of Sn−3.0Ag solder are $Sn_{21}Cl_{16}(OH)_{14}O_6$, SnO_2, and SnO.

PVC fire smoke contains a large number of HCl, H_2O, and carbon particles, which has strong hygroscopicity. When deposited on Sn−3.0Ag solder surface, it is easy to absorb inorganic salts and water vapor in the air and leads to the formation of electrolyte solution on the solder surface. In addition, Sn−3.0Ag solder is composed of Sn-rich

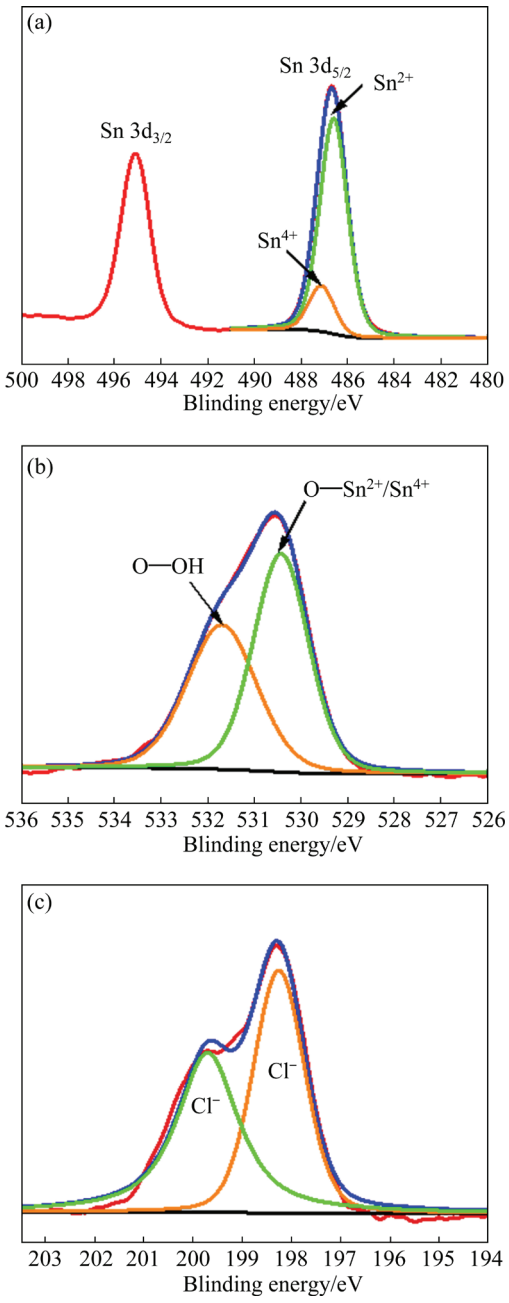

Fig. 8 XPS spectra for detected elements of corrosion products for Sn−3.0Ag solder in PVC fire smoke environment at 323.15 K: (a) Sn 3d; (b) O 1s; (c) Cl 2p

phase and intermetallic compound of Ag_3Sn [31]. And potential differences exist between the Sn-rich phase and Ag_3Sn or carbon particles, forming a corrosive galvanic cell and resulting in the electrochemical corrosion of Sn−3.0Ag solder [35,36]. As HCl is dissolved in the electrolyte solution, the solution is acidic. Thus, the hydrogen evolution reaction occurs at the cathode. In addition, since oxygen has a higher equilibrium potential than hydrogen, oxygen is easy to diffuse onto the thin

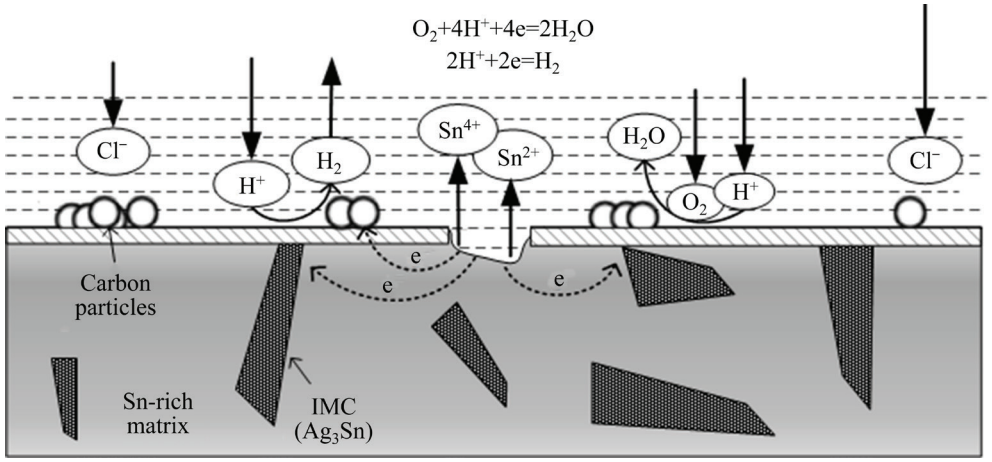

Fig. 9 Corrosion mechanism of Sn−3.0Ag solder in PVC fire smoke environment

liquid film on the cathode surface [37,38]. Therefore, the cathode is also accompanied by an oxygen abstraction reaction (Fig. 9) as follows:

$$O_2+4H^++4e=2H_2O \quad (4)$$

$$2H^++2e=H_2 \quad (5)$$

The anodic reaction is mainly the dissolution of the Sn-rich phase, and the reaction formula is as follows:

$$Sn=Sn^{2+}+2e \quad (6)$$

$$Sn^{2+}=Sn^{4+}+2e \quad (7)$$

Subsequently, Sn^{2+} reacts with H_2O to form $Sn(OH)_2$ and then further dehydrates to form SnO. Sn^{4+} reacts with H_2O to produce $Sn(OH)_4$, and then dehydrates to form SnO_2:

$$Sn^{2+}+2H_2O=Sn(OH)_2+2H^+ \quad (8)$$

$$Sn(OH)_2=SnO+H_2O \quad (9)$$

$$Sn^{4+}+4H_2O=Sn(OH)_4+4H^+ \quad (10)$$

$$Sn(OH)_4=SnO_2+2H_2O \quad (11)$$

In addition, the Sn-rich phase reacts directly with H_2O to form $Sn(OH)_4$:

$$Sn+4H_2O=Sn(OH)_4+4H^++4e \quad (12)$$

Due to the erosion of Cl^-, most Sn-rich phases are directly eroded by Cl^- to form compounds, $Sn_{21}Cl_{16}(OH)_{14}O_6$:

$$21Sn+14H^++10O_2+16Cl^-= Sn_{21}Cl_{16}(OH)_{14}O_6+2e \quad (13)$$

The corrosion degree of Sn−3.0Ag solder mainly involves an electrochemical reaction process. With the increase of temperature, the electrolyte solution resistance decreases, the oxygen diffusion rate and the cathode reaction rate increase. Therefore, temperature plays a crucial role in determining the corrosion degree of Sn−3.0Ag solder. Higher temperatures accelerate the corrosion degree of Sn−3.0Ag solder.

4 Conclusion

(1) Temperature has a great influence on the corrosion behavior of Sn−3.0Ag lead-free solder in PVC fire smoke environment. With the increase of temperature from 283.15 to 323.15 K, the mass-loss of Sn−3.0Ag solder increases from (22.09±2.01) to (44.66±1.20) g/m^2. In addition, the mass-loss variation with temperature is in accordance with Arrhenius law.

(2) Small patches of corrosion products appear on Sn−3.0Ag lead-free solder surface in PVC fire smoke environment at 283.15 K. As the temperature increases, the corrosion products show a trend of first increasing and then thickening in the superposition growth mode. At 323.15 K, the corrosion products densely and thickly cover Sn−3.0Ag solder surface.

(3) The corrosion process of Sn−3.0Ag lead-free solder in PVC fire smoke environment is an electrochemical corrosion. Reactions of hydrogen evolution and oxygen abstraction occur in the cathode, and the Sn-rich phase is dissolved at the anode. The corrosion products are mainly $Sn_{21}Cl_{16}(OH)_{14}O_6$, with a small amount of SnO_2 and SnO.

CRediT authorship contribution statement

Qian LI: Conceptualization, Data curation, Methodology, Writing − Original draft, Writing − Reviewing & editing; **Jin LIN:** Conceptualization,

Methodology, Project administration, Writing − Reviewing & editing; **Meng-ke ZHAO:** Formal analysis, Investigation, Validation; **Chang-hai LI:** Formal analysis, Investigation; **Shou-xiang LU:** Funding acquisition, Project administration, Resources, Supervision.

Declaration of competing interest

The authors declare that they have no known competing financial interests or personal relationships that could have appeared to influence the work reported in this paper.

Data availability statements

The authors declare that the data supporting the findings of this study are available within the article.

Acknowledgments

The authors gratefully acknowledge financial support by the National Natural Science Foundation of China (No. 52206180) and the Fundamental Research Funds for the Central Universities, China (No. WK2320000050).

References

[1] ILLES B, CHOI H, HURTONY T, DUSEK K, BUSEK D, SKWAREK A. Suppression of Sn whisker growth from SnAgCu solder alloy with TiO_2 and ZnO reinforcement nano-particles by increasing the corrosion resistance of the composite alloy [J]. Journal of Materials Research and Technology, 2022, 20: 4231−4240.

[2] KAVITHA M, MAHMOUD Z H, KISHORE K H, PETROV A M, LEKOMTSEV A, ILIUSHIN P, ZEKIY A O, SALMANI M. Application of Steinberg model for vibration lifetime evaluation of Sn−Ag−Cu−based solder joints in power semiconductors [J]. IEEE Transactions on Components, Packaging and Manufacturing Technology, 2021, 11(3): 444−450.

[3] CHEN Jian-xun, ZHAO Xing-ke, ZOU Xu-chen, HUANG Ji-hua, HU Hai-chun, LUO Hai-lian. Characterization of Cu3P phase in Sn3.0Ag0.5Cu0.5P/Cu solder joints [J]. International Journal of Minerals, Metallurgy, and Materials, 2014, 21: 65−70.

[4] ZHAO Hui, SUN Xu, HAO Long, WANG Jian-qiu, YANG Jing-mei. Corrosion evolution of high-temperature formed oxide film on pure Sn solder substrate [J]. Transactions of Nonferrous Metals Society of China, 2022, 32(12): 3998−4013.

[5] JELLESEN M S, MINZARI D, RATHINAVELU U, MOLLER P, AMBAT R. Investigation of electronic corrosion at device level [J]. ECS Trans, 2010, 25(30): 1−14.

[6] WANG Xi, ZHANG Liang, WANG Xiao, GUO Yong-huan, SUN Lei, LIU Ying-xia, CHEN Chen, LU Xiao. Growth behavior and reliability of interfacial IMC for Sn58Bi/Cu and Sn58Bi−AlN/Cu solder joints applied in IGBT modules [J]. Journal of Materials Research and Technology, 2022, 21: 4263−4280.

[7] VUONG B X, VU N S H, MANH T D, VAKA M, DU D X, NAM N D. Role of cerium in microstructure and corrosion properties of Sn−1.0 Ag solder alloys [J]. Materials Letters, 2018, 228: 309−313.

[8] WU Ming, WANG Shan-lin, SUN Wen-jun, HONG Min, CHEN Yu-hua, KE Li-ming. Fracture pattern evolution of SnAgCu−SnPb mixed solder joints at cryogenic temperature [J]. Transactions of Nonferrous Metals Society of China, 2021, 31(9): 2762−2772.

[9] RASHIDI R, NAFFAKH-MOOSAVY H. Metallurgical, physical, mechanical and oxidation behavior of lead-free chromium dissolved Sn−Cu−Bi solders [J]. Journal of Materials Research and Technology, 2021, 13: 1805−1825.

[10] WANG Zheng-hong, CHEN Chuan-tong, JIU Jin-ting, NAGAO S, NOGI M, KOGA H, ZHANG Hao, ZHANG Gong, SUGANUMA K. Electrochemical behavior of Zn−*x*Sn high-temperature solder alloys in 0.5 M NaCl solution [J]. Journal of Alloys and Compounds, 2017, 716: 231−239.

[11] CHANTARAMANEE S, SUNGKHAPHAITOON P. Combined effects of Bi and Sb elements on microstructure, thermal and mechanical properties of Sn−0.7Ag−0.5Cu solder alloys [J]. Transactions of Nonferrous Metals Society of China, 2022, 32(10): 3301−3311.

[12] LAO Xiao-dong, CHENG Cong-qian, MIN Xiao-hua, ZHAO Jie, ZHOU Da-yu, WANG Li-hua, LI Xiao-gang. Corrosion and leaching behaviors of Sn-based alloy in simulated soil solutions [J]. Transactions of Nonferrous Metals Society of China, 2016, 26(2): 581−588.

[13] LI Shuai, WANG Xing-xing, LIU Zhong-ying, JIU Yong-tao, ZHANG Shu-ye, GENG Jin-feng, CHEN Xiao-ming, WU Sheng-jin, HE Peng, LONG Wei-min. Corrosion behavior of Sn-based lead-free solder alloys: A review [J]. Journal of Materials Science: Materials in Electronics, 2020, 31: 9076−9090.

[14] MA Hao-ran, KUNWAR A, LIU Zhi-yuan, CHEN Jun, WANG Yun-peng, HUANG Ming-liang, ZHAO Ning, MA Hai-tao. Shielding effect of Ag_3Sn on growth of intermetallic compounds in isothermal heating and cooling during multiple reflows [J]. Journal of Materials Science: Materials in Electronics, 2018, 29: 4383−4390.

[15] TUNTHAWIROON P, KANLAYASIRI K. Effects of Ag contents in Sn–*x*Ag lead-free solders on microstructure, corrosion behavior and interfacial reaction with Cu substrate [J]. Transactions of Nonferrous Metals Society of China, 2019, 29(8): 1696−1704.

[16] WANG Zheng-hong, CHEN Chuan-tong, LIU Jian-chun, ZHANG Gong, SUGANUMA K. Corrosion mechanism of Zn−30Sn high-temperature, lead-free solder in neutral NaCl solution [J]. Corrosion Science, 2018, 140: 40−50.

[17] WANG Ming-na, WANG Jian-qiu, KE Wei. Corrosion behavior of Sn−3.0Ag−0.5Cu lead-free solder joints [J]. Microelectronics Reliability, 2017, 73: 69−75.

[18] WATTS JR J M. Nonthermal fire damage [J]. Fire Technology, 2001, 37(2): 107.

[19] NEWMAN J S, YEE G G, SU P, XIN Yi-bing, REN Ning. Smoke damage potentials in industrial fire applications [J]. Fire Technology, 2014, 50: 1437−1458.

[20] LI De-zhi, CONWAY P P, LIU Chang-qing. Corrosion characterization of tin–lead and lead free solders in 3.5 wt.% NaCl solution [J]. Corrosion Science, 2008, 50: 995−1004.
[21] YOKOYAMA K I, NOGAMI A, SAKAI J I. Creep corrosion cracking of Sn−3.0Ag and Sn−0.5 Cu solder alloys in NaCl solution [J]. Corrosion Science, 2014, 86: 142−148.
[22] OSORIO W R, FREITAS E S, SPINELLI J E, GARCIA A. Electrochemical behavior of a lead-free Sn−Cu solder alloy in NaCl solution [J]. Corrosion Science, 2014, 80: 71−81.
[23] HEAKAL F E T, FEKRY A M, GHONEIM A A. Corrosion characterization of new tin–silver binary alloys in nitric acid solutions [J]. Corrosion Science, 2008, 50(6): 1618−1626.
[24] LI Xue-zheng, MA Yong, ZHOU Wei, WU Ping. Effects of nanoscale Cu_6Sn_5 particles addition on microstructure and properties of SnBi solder alloys [J]. Materials Science and Engineering A, 2017, 684: 328−334.
[25] SHARMA A, DAS S, DAS K. Electrochemical corrosion behavior of CeO_2 nanoparticle reinforced Sn−Ag based lead free nanocomposite solders in 3.5 wt.% NaCl bath [J]. Surface and Coatings Technology, 2015, 261: 235−243.
[26] QIAO Chuang, WANG Ming-na, HAO Long, JIANG Xiao-lin, LIU Xia-he, THEE C, AN Xi-zhong. In-situ EIS study on the initial corrosion evolution behavior of SAC305 solder alloy covered with NaCl solution [J]. Journal of Alloys and Compounds, 2021, 852: 156953.
[27] DICKINSON P R. Evolving fire retardant material issues: A cable manufacturer's perspective [J]. Fire Technology, 1992, 28: 345−368.
[28] ARTIGAS A, MONSALVE A, SIPOS K, BUSTOS O, MENA J, SECO R, GARZA-MONTES-DE-OCA N. Development of accelerated wet–dry cycle corrosion test in marine environment for weathering steels [J]. Corrosion Engineering, Science and Technology, 2015, 50(8): 628−632.
[29] BENHIBA F, BENZEKRI Z, GUENBOUR A, TABYAOUI M, BELLAOUCHOU A, BOUKHRIS S, OUDDA H, WARAD I, ZARROUK A. Combined electronic/atomic level computational, surface (SEM/EDS), chemical and electrochemical studies of the mild steel surface by quinoxalines derivatives anti-corrosion properties in 1 mol/L HCl solution [J]. Chinese Journal of Chemical Engineering, 2020, 28(5): 1436−1458.
[30] ABIOLA O K, TOBUN Y. COCOS NUCIFERA L. Water as green corrosion inhibitor for acid corrosion of aluminium in HCl solution [J]. Chinese Chemical Letters, 2010, 21(12): 1449−1452.
[31] LI Qian, LIU Xu-fei, LU Shou-xiang. Physics, Corrosion behavior assessment of tin-lead and lead free solders exposed to fire smoke generated by burning polyvinyl chloride [J]. Materials Chemistry and Physics, 2018, 212: 298−307.
[32] WANG Ming-na, WANG Jian-qiu, FENG Hao, KE Wei. Effect of Ag_3Sn intermetallic compounds on corrosion of Sn−3.0Ag−0.5Cu solder under high-temperature and high-humidity condition [J]. Corrosion Science, 2012, 63: 20−28.
[33] ZHONG Xian-kang, ZHANG Guo-an, QIU Yu-bing, CHEN Zhen-yu, GUO Xing-peng. Effect of citrate ions on the electrochemical migration of tin in thin electrolyte layer containing chloride ions [J]. Corrosion Science, 2016, 112: 393−401.
[34] KWOKA M, OTTAVIANO L, PASSACANTANDO M, SANTUCCI S, CZEMPIK G, SZUBER J. XPS study of the surface chemistry of L-CVD SnO_2 thin films after oxidation [J]. Thin Solid Films, 2005, 490(1): 36−42.
[35] SATIZABAL L M, COSTA D, MORAES P B, BORTOLOZO A D, OSORIO W R. Microstructural array and solute content affecting electrochemical behavior of SnAg and SnBi alloys compared with a traditional SnPb alloy [J]. Materials Chemistry and Physics, 2019, 223: 410−425.
[36] ELIAS A L P, KOIZUMI M S, ORTIZ E L, RODRIGUES J F Q, BORTOLOZO A D, OSORIO W R, da SILVA PADILHA G. Corrosion behavior of an Al−Si casting and a sintered Al/Si composite immersed into biodiesel and blends [J]. Fuel Processing Technology, 2020, 202: 106360.
[37] EVANS U R. Electrochemical mechanism of atmospheric rusting [J]. Nature, 1965, 206: 980−982.
[38] EVANS U R. The corrosion and oxidation of metals [M]. 1st Ed. Edward Arnold Ltd, 1960, 401.

聚氯乙烯火灾烟气环境中无铅焊料腐蚀动力学预测模型

李 倩，林 锦，赵梦珂，黎昌海，陆守香

中国科学技术大学 火灾科学国家重点实验室，合肥 230026

摘 要：采用质量损失法研究聚氯乙烯火灾烟气环境中 283.15~323.15 K 温度范围内无铅 Sn−3.0Ag 焊料的腐蚀动力学、表面微观结构和腐蚀机理。结果表明，随着温度从 283.15 K 升高到 323.15 K，Sn−3.0Ag 焊料的质量损失从(22.09±2.01) g/m^2 增加到(44.66±1.20) g/m^2。此外，腐蚀动力学符合阿伦尼乌斯定律。Sn−3.0Ag 焊料表面腐蚀产物呈叠加生长趋势。在 283.15 K，Sn−3.0Ag 焊料的表面出现大量的腐蚀产物。Sn−3.0Ag 无铅焊料的腐蚀过程为电化学腐蚀，阴极发生析氢和吸氧反应，阳极发生富锡相的溶解。腐蚀产物为 $Sn_{21}Cl_{16}(OH)_{14}O_6$、$SnO_2$ 和 SnO。

关键词：腐蚀；预测模型；Sn−3.0Ag 焊料；火灾烟气；温度

(Edited by Bing YANG)